Cerebral Cortex, December 2015;25: 4854–4868

doi: 10.1093/cercor/bhv202
Advance Access Publication Date: 24 September 2015
Original Article

ORIGINAL ARTICLE

Characterizing VIP Neurons in the Barrel Cortex of VIPcre/tdTomato Mice Reveals Layer-Specific Differences

Alvar Prönneke, Bianca Scheuer, Robin J. Wagener, Martin Möck, Mirko Witte, and Jochen F. Staiger

Institute for Neuroanatomy, Universitätsmedizin Göttingen, Georg-August-Universität, Göttingen D-37075, Germany

Address correspondence to Alvar Prönneke, Institute for Neuroanatomy, Universitätsmedizin Göttingen, Georg-August-Universität, Kreuzbergring 36, D-37075 Göttingen, Germany. Email: alvar.proenneke@med.uni-goettingen.de; Jochen F. Staiger. Email: jochen.staiger@med.uni-goettingen.de.

Alvar Prönneke and Bianca Scheuer contributed equally to this work.

Jochen F. Staiger and Mirko Witte contributed equally to this work.

Abstract

Neocortical GABAergic interneurons have a profound impact on cortical circuitry and its information processing capacity. Distinct subgroups of inhibitory interneurons can be distinguished by molecular markers, such as parvalbumin, somatostatin, and vasoactive intestinal polypeptide (VIP). Among these, VIP-expressing interneurons sparked a substantial interest since these neurons seem to operate disinhibitory circuit motifs found in all major neocortical areas. Several of these recent studies used transgenic *Vip-ires-cre* mice to specifically target the population of VIP-expressing interneurons. This makes it necessary to elucidate in detail the sensitivity and specificity of Cre expression for VIP neurons in these animals. Thus, we quantitatively compared endogenous tdTomato with *Vip* fluorescence in situ hybridization and αVIP immunohistochemistry in the barrel cortex of VIPcre/tdTomato mice in a layer-specific manner. We show that VIPcre/tdTomato mice are highly sensitive and specific for the entire population of VIP-expressing neurons. In the barrel cortex, approximately 13% of all GABAergic neurons are VIP expressing. Most VIP neurons are found in layer II/III (~60%), whereas approximately 40% are found in the other layers of the barrel cortex. Layer II/III VIP neurons are significantly different from VIP neurons in layers IV–VI in several morphological and membrane properties, which suggest layer-dependent differences in functionality.

Key words: barrel cortex, cortical interneurons, GABA, vasoactive intestinal polypeptide, *Vip-ires-cre*

Introduction

Cortical interneurons play an important role in controlling and shaping excitation in cortical circuits (McBain and Fisahn 2001; Pouille and Scanziani 2001; Wehr and Zador 2003; Klausberger and Somogyi 2008; Haider and McCormick 2009). They are heterogeneous in morphology and electrophysiological characteristics as well as molecular profiles, which proved to be a major obstacle in past classification attempts (Cauli et al. 2000; Markram et al. 2004; Ascoli et al. 2008; DeFelipe et al. 2013). Today, however, the population of inhibitory interneurons is generally viewed as subgroups based on the distinct expression of certain proteins. These nonoverlapping subgroups are parvalbumin (PV), somatostatin (SOM), and serotonin receptor 3a (5HT3aR)-expressing inhibitory interneurons. Roughly 30% of 5HT3aR interneurons also express vasoactive intestinal polypeptide (VIP; Lee et al. 2010; Rudy et al. 2011; Zeisel et al. 2015).

Cortical VIP neurons are key elements in neurovascular coupling (Cauli et al. 2004) and in the regulation of neuronal energy metabolism (Magistretti et al. 1998). In terms of cortical circuitry, it has been repeatedly reported that VIP neurons preferentially target several other types of inhibitory interneurons (Staiger et al. 2004b; David et al. 2007; Pfeffer et al. 2013), thus mediating disinhibition by releasing excitatory principal neurons from inhibition. The disinhibitory circuit motif involving the VIP-to-SOM connectivity has now been functionally characterized in the visual (Fu et al. 2014; Zhang et al. 2014), the auditory (Pi et al. 2013), and the primary somatosensory (barrel) cortex (Lee et al. 2013).

These functional studies used genetically engineered *Vip-ires-cre* knock-in mice (Taniguchi et al. 2011), in which the expression of the recombinase Cre is dependent on the expression of VIP to exclusively target VIP neurons. The characterization of the specificity of Cre expression in VIP cells in *Vip-ires-cre* mice has so far been restricted to the upper layers of the barrel cortex and a low number of cells. Results showed a 91.5% specificity of Cre expression for VIP (Taniguchi et al. 2011). It remains unclear, however, whether this high specificity is consistent throughout the whole barrel cortex and its different layers. It also was important to verify that these neurons are indeed GABAergic since it has been reported that some interneurons could be excitatory (Peters and Harriman 1988; Wouterlood et al. 2008). Apart from these neurochemical properties, morphological and electrophysiological properties of individual VIP neurons in mice are also still ill-defined.

Thus, we crossed *Vip-ires-cre* mice (Taniguchi et al. 2011) with tdTomato-expressing Ai9 mice (Madisen et al. 2010). To analyze VIP expression independently of Cre, we performed fluorescence in situ hybridization (FISH) using probes for the RNA of *Vip*, and immunohistochemistry (IHC) with VIP antibodies (ABs) in the barrel cortex of adult VIPcre/tdTomato mice. This allowed for a quantification of the co-localization of Cre-driven and FISH- or IHC-derived fluorescence. Furthermore, we quantified the distribution of VIP neuron somata in a layer-specific as well as independent manner. Finally, we targeted individual VIP neurons in all layers of the barrel cortex for whole-cell patch-clamp recordings and biocytin filling in order to obtain their electrophysiological and morphological characteristics.

In this study, we not only confirm the high specificity of VIPcre/tdTomato mice for VIP neurons, but also present a substantial new insight into the distribution, electrophysiology, and morphology of VIP neurons across all layers of the barrel cortex in adult mice. VIP neurons express the inhibitory marker glutamate decarboxylase (GAD), but never the excitatory marker vesicular glutamate transporter 1 (vGlut1), PV, or SOM. The majority of VIP neurons are located in layer II/III (~60%), whereas approximately 40% are found in the other layers of the barrel cortex. VIP neurons in layer II/III show significant differences from those found in layer IV–VI in several morphological and electrophysiological characteristics. Most importantly, layer II/III VIP neurons virtually restrict their dendritic trees to layers I and II/III, but spread their axons across all layers of the barrel cortex. In contrast, layer IV–VI VIP neurons extend their dendrites throughout all layers, while their axons are largely restricted to layers V and VI.

Materials and Methods

Animals

We crossed homozygous *Vip-ires-cre* (VIP$^{tm1(cre)Zjh}$, The Jackson Laboratory, Bar Harbor, USA) mice with homozygous *Ai9* mice (Madisen et al. 2010; B6.Cg-*Gt(ROSA)26Sor*$^{tm9(CAG-tdTomato)Hze}$/J, The Jackson Laboratory). Offspring (20–30 weeks old for IHC and FISH; 24–36 days old for electrophysiological experiments) heterozygous for VIPcre/tdTomato, from the breeding facility of the University Medical Center Göttingen (Göttingen, Germany), were used in this study. All experimental procedures were performed in accordance with German laws on animal research (TierSchG und TierSchVersV 2013).

Fixation and Tissue Processing

The perfusion was done transcardially with 10% sucrose, followed by 150 mL of 4% paraformaldehyde in 0.1 M phosphate buffer (PB), pH 7.4. Brains were dissected out of the skull and postfixed for 2 h. Forebrain blocks for immunostaining were sectioned in the coronal plane on a vibratome (VT 1200S, Leica, Wetzlar, Germany) at 40 µm thickness. Brains for FISH underwent cryoprotection and were coronally sectioned with a cryostat (Cryo-Star HM560 MW, Thermo Fisher Scientific, Walldorf, Germany) at 40 µm thickness.

Immunohistochemistry

The sections were rinsed in Tris buffer (TB), 0.05 M Tris-buffered saline (TBS), and TBS containing 0.5% Triton X-100 (TBST; 2× 15 min each), all pH 7.6, and blocked with 10% normal goat serum (in TBST) for 90 min. The sections were then incubated for 48–72 h at 4 °C with one of the following primary ABs: rb-α-VIP 43841 (Abcam, Cambridge, UK) 1 : 1000, rb-α-VIP ImmunoStar 722001/20077 (ImmunoStar, Dietzenbach, Germany) 1 : 2000, rb-α-PV 25 (Swant, Marly, Switzerland) 1 : 5000, or rb-α-SOM T-4103 (Bachem, Bubendorf, Switzerland) 1 : 5000. The sections were subsequently rinsed in TBST (4× 15 min) and then incubated in Alexa Fluor 488-conjugated AB raised against rabbit IgG (goat anti-rabbit, 1 : 500, Life Technologies, Darmstadt, Germany) at room temperature (RT). After several washes with TBST, the sections were incubated with DAPI (1 : 1000, Life Technologies) and finally mounted in Aqua Poly-Mount (Polyscience, Warrington, USA).

Fluorescence In Situ Hybridization

FISH was performed with cRNA probes. The probes were generated from custom-manufactured plasmids (vector backbone: pGMT easy, Promega or pCR-Blunt II-TOPO, Invitrogen) containing cDNA inserts of the respective genes. Primer for DNA inserts: *Gad1* (320 bp) forward primer (FP): GGCACGACTGTTTACGGAGC, reverse primer (RP): GCCTTGTCCCCGGTGTCATA; *Slc17a7* (also known as *vGlut1*; 719 bp; Allen Brain Atlas Riboprobe ID: RP_050310_01_B09) FP: CAGAGCCGGAGGAGATGA; RP: TTCCCTCAGAAACGCTGG, (nested 296 bp) FPnested: GCTGGCAGTGACGAAAGTGA, RPnested: TGAGAGGGAAAGAGGGCTGG; *Vip* (527 bp; Allen Brain Atlas Riboprobe ID: RP_070116_02_E09) FP: CCTGGCATTCCTGATACTCTTC, RP: ATTCTCTGATTTCAGCTCTGCC, (nested 367 bp) FPnested: CTGTTCTCTCAGTCGCTGGC, RPnested: GCTTTCTGAGGCGGGTGTAG; *Pvalb* (434 bp) FP: ACGGCAAGATTGGGGTTGAA, RP: TCTCCTTGTGGGAAAGGTGC); *Sst* (514 bp; Allen Brain Atlas Riboprobe ID: RP_081204_01_A03) FP: ACGCTACCGAAGCCGTC; RP: GGGGCCAGGAGTTAAGGA. The plasmids were linearized with the appropriate restriction enzymes and served as templates for in vitro transcription using a DIG RNA labeling kit (Roche Applied Science, Mannheim, Germany). After blocking endogenous peroxidase with 1% H_2O_2 in methanol, sections were quenched with 0.2 M HCl, digested with proteinase

K (20 µg/mL, Roche) in Tris–HCl/EDTA (50 mM/5 mM, pH 8), and finally postfixed in 4% PFA. Between all steps, sections were rinsed in PBS. After a treatment with 0.25% acetic anhydride (2.4/µL per mL 0.1 M triethanolamine/HCl) for 10 min, sections were rinsed twice in 2× standard saline citrate (1× SSC: 0.15 M NaCl, 0.015 M sodium citrate, pH 7.0) and pretreated for 15 min in hybridization buffer (HB; 50% formamide, 4× SSC, 250 µg/mL of denaturated salmon sperm DNA, 100 µg/mL of tRNA, 5% dextransulfate, and 1% Denhardt's solution) diluted 1 : 1 with 2× SSC. The procedure was followed by 1 h of prehybridization at 55 °C in pure HB. DIG-labeled RNA probes (200 ng/mL) were hybridized overnight at 55 °C. The next morning, stringency washes were done in 2× SSC (2× 15 min, RT), 2× SSC containing 50% formamide (2× 30 min, at 65 °C), and 2× SSC (2× 5 min, at 65 °C). After RNase A treatment (4 µg/mL), the sections were rinsed again in 2× SSC (5 min, RT), 2× SSC containing 50% formamide (30 min, 65 °C), 0.1× SSC containing 50% formamide (15 min, at 65 °C), and finally with 0.1× SSC (2× 15 min, at 65 °C). The tissue was blocked with 4% sheep serum and 0.5% blocking agent (PerkinElmer). Hybridized probes were then incubated overnight with anti-DIG Fab fragments conjugated with peroxidase (raised in sheep; Roche) diluted 1 : 2000 in blocking agent containing 0.01 M TBS, pH 7.5. The AB signal was amplified using a Tyramide Signal Smplification Kit (TSA Biotin System NEL700001KT; PerkinElmer). Biotinyl tyramide working solution was incubated for 2 h. After rinsing in TBS, Streptavidin Alexa Fluor 488 (Molecular Probes; diluted 1 : 400 in TBS, 15 min) was used for detection of the covalently attached biotin.

Subsequent immunoamplification of the tdTomato signal was done with an anti-DsRed AB (anti-rabbit; 1 : 250; Clontech Laboratories, Mountainview, CA, USA) according to the standard IHC protocol (see above), but omitting the Triton treatment. The secondary AB was coupled with Alexa 546 (1 : 500; Life Technologies).

Image Acquisition and Data Analysis

All sections were imaged using an upright epi-fluorescence microscope (AxioImager.M2, Zeiss, Jena, Germany) using structured illumination (ApoTome, Zeiss). The set-up was controlled by the software Neurolucida (MBF Bioscience, Colchester, VT, USA). The barrel cortex and its layers were identified in acquired image stacks by DAPI stainings. Layer borders were determined according to the following cytoarchitectonic criteria: Layer I shows the lowest cell density, which easily distinguishes it from layer II/III. Layer IV can be identified by its cell-dense barrels. Layer V is characterized by a low density of large somata, whereas layer VI shows a high density of smaller somata that clearly separates these layers. Layer V can be subdivided into layer Va and b since layer Va consists of even fewer cell bodies (engaging approximately a third of layer V; Schubert et al. 2006). We analyzed 18 615 tdTomato-positive cells and 38 440 cells stained by IHC for PV (5739) or SOM (4089) and FISH with probes for *Pvalb* (7539), *Sst* (5514), and *Gad1* (15559) in 150 sections from 12 animals. The density of cells was determined by normalizing data derived from the barrel cortex in each section to mm^3. Thus, numbers for all cells or for cells from individual layers were scaled to 1 mm^3 cortical tissue (including all layers; i.e., cells/mm^3 cortex). For a detailed comparison of VIP cell density between layers, we used the number of cells within the given layer scaled to 1 mm^3 of tissue of the respective layer (i.e., cells/mm^3 layer X). For the results of the bin-size analysis, we used 20 bins; thus, the unit is 1/20th mm^3 which is given as cells/0.05 mm^3 (see Supplementary Fig. 1 for details).

In Vitro Electrophysiology

VIPcre/tdTomato mice were deeply anesthetized with isoflurane and decapitated. Thalamocortical slices (300 µm; Porter et al. 2001) containing the primary somatosensory (barrel) cortex were cut using a vibratome (Leica VT1200S). The cold (4 °C) cutting solution contained (in mM): 75 sucrose, 87 NaCl, 2.5 KCl, 0.5 $CaCl_2$, 7.0 $MgCl_2$, 26 $NaHCO_3$, 1.25 NaH_2PO_4, and 10 glucose, continuously equilibrated with 95% O_2 and 5% CO_2, pH 7.4. Slices were incubated for 0.5–1 h at 34 °C prior to recording in extracellular solution [artificial cerebro-spinal fluid (ACSF)] of the following composition (in mM): 125 NaCl, 2.5 KCl, 2 $CaCl_2$, 1 $MgCl_2$, 26 $NaHCO_3$, 1.25 NaH_2PO_4, and 25 glucose, pH 7.4 when equilibrated with 95% O_2 and 5% CO_2.

Slices were transferred to a fixed-stage recording chamber in an upright microscope (Axio Examiner, Zeiss) and continuously perfused at a rate of 2 mL/min with ACSF. All experiments were performed at 32 °C.

The barrel field was visualized at low magnification (×2.5) under bright-field illumination. Target neurons were identified by tdTomato fluorescence using a ×40 water immersion objective (×40/0.75 W, Olympus, Germany). For whole-cell patch-clamp recordings, filamented borosilicate glass capillaries (Science Products, Hofheim, Germany) of 5–8 MΩ resistances were filled with (in mM): 135 K-gluconate, 5 KCl, 10 HEPES, 0.5 EGTA, 4 Mg-ATP, 0.3 Na-GTP, 10 phosphocreatine phosphate, and 0.3–0.5% biocytin. Membrane potentials were not corrected for a liquid junction potential of approximately 16 mV. Membrane potentials were recorded using an SEC-05L amplifier (npi electronics, Tamm, Germany) in discontinuous current-clamp mode with a switching frequency of 50 kHz, filtered at 3 kHz, and digitized at 10–25 kHz using a CED Power1401 (CED Limited, Cambridge, UK). Access resistance was monitored and compensated if changes appeared. Recordings during which the access resistance could not be compensated were discarded. Data were collected, stored, and analyzed with the Signal 5 software (CED Limited). Passive and active properties of a neuron were determined immediately after reaching whole-cell configuration by applying 1 s long hyperpolarizing or depolarizing rectangular current pulses of varying strength at resting membrane potential.

Staining of Biocytin-Filled Cells

Staining of biocytin-filled cells has previously been described in detail (Staiger et al. 2004a, 2014). In brief, after recording slices were fixed in 4% formaldehyde (in PB) at 4 °C for 12–20 h. To stop fixation, the tissue was rinsed extensively with PB, including an intermediate step with 1% H_2O_2 (in PB) to block endogenous peroxidase activity. Next, slices were incubated in a cryoprotectant (25% saccharose and 10% glycerol in 0.01 M PB) for 1 h. They were freeze–thawed 3 times over liquid nitrogen. After 3 rinses in PB, the slices were incubated overnight with Avidin-Biotin Complex (ABC; 1 : 200; Vector, Burlingame, CA, USA) at 4 °C. Subsequently, 1 mg/mL of 3,3′-diaminobenzidine (DAB; Sigma, Deisenhofen, Germany) was preincubated for 10 min and the peroxidase was revealed by starting the reaction with 0.01% H_2O_2. The reaction was stopped by rinsing with PB. To intensify the reaction product, sections were dehydrated and cleared in xylene overnight and then rehydrated and incubated in 1.4% silver nitrate at 56 °C for 30 min, followed by 0.2% gold chloride at RT for 10 min, and fixed with 5% sodium thiosulfate for 5 min. The barrel field was visualized by cytochrome oxidase histochemistry.

Reconstruction of Biocytin-Filled Neurons

Neurons with consistently intense staining of neurites and no obvious truncation of processes were reconstructed using live

digital images acquired by a digital camera (CX9000, MBF Bioscience) mounted on a microscope (Eclipse 80i, Nikon, Ratingen, Germany) with a ×63 oil immersion objective (NA = 1.4) and connected to a computer running Neurolucida (MBF Bioscience). Dendritic processes were distinguished from axonal structures by their diameter, fine structure, and branching pattern (see Supplementary Fig. 2 for details).

Data Analysis and Statistics

Electrophysiological data were analyzed using custom-written scripts for Signal 5. Most of the passive properties were analyzed using averages of 10 responses to a hyperpolarizing current pulse of −10 pA. The membrane time constant (τ) was determined by fitting an exponential to the averaged membrane potential response ($f(x) = Ae^{-x/\tau} + B$; A = maximum amplitude, B = membrane potential at the maximum amplitude of response; $R^2 > 0.9$). Input resistance was determined according to Ohm's law using the maximum amplitude of the membrane potential response and the amplitude of the injected current. The sag index is an indicator of slow inward rectification. It was calculated by comparing the input resistance at the maximum amplitude to that at steady state (averaged membrane potential toward the end of the stimulus). Differences are given as percentages. Fast inward rectification (rectification index, RI) was measured by comparing the maximal membrane potential changes as responses to current pulses of −10 pA with those to −100 pA. Linearity (response to −10 pA is 10% of that to −100 pA) suggests that the deflection depends exclusively on passive membrane properties. An increase in the percentage indicates involvement of fast inward rectification. For clarity, we subtracted 10 from the resulting values, and thus no fast inward rectification is set to 0. Firing threshold, time to peak, half width, and amplitude (measured from firing threshold to peak) of action potentials were analyzed at action potentials evoked at rheobase. The amplitude of afterhyperpolarizations (AHP) was determined by measuring the difference in voltage from firing threshold to maximum deflection of the repolarization. The time to peak of AHP was measured from the time point the repolarization of the action potential crossed the firing threshold to the maximum amplitude of the AHP.

Properties of reconstructed neurons were quantified with Neurolucida Explorer (MBF Bioscience). Data were not corrected for tissue shrinkage. However, from several measurements, we estimated the shrinkage to be around 10–15% in the x-/y-axes and 40–60% in the z axis. The horizontal spread of dendritic and axonal fibers was determined by measuring the maximum distance of structures parallel to the pial surface, whereas the vertical spread was measured perpendicular to the pial surface.

To superimpose multiple reconstructions and show the distribution of neuronal processes as a population average, reconstructed neurons were registered into one file using defined layer borders (average of layers identified by DAPI stainings of 150 sections through the barrel cortex) as a reference, somata aligned at the same horizontal level, and all fibers plotted as one binary image. This was filtered using a Gaussian filter with a comparable radial sigma (20 at 300 dpi) for all structures and a color look-up-table ranging from cold (blue and green for white to light gray) to warm colors (yellow and red for dark gray to black) was applied to the resulting grayscale image. This was then merged with the original black and white image and resulted in heat maps visualizing areas of highest density of axonal and dendritic trees.

For statistical comparisons, data were tested for normality (Shapiro–Wilk test) and equal variance. If both passed, a one-way Student's t-test was used. If one or both failed, a Mann–Whitney rank sum test was used. The distribution of tdTomato-positive cell bodies was tested for significant differences using a Kruskal–Wallis one-way analysis of variance (ANOVA) on ranks since the Shapiro–Wilk test for normality failed. A post hoc Tukey test as an all pairwise multiple comparison procedure to identify significant different bins was applied. All values are given as mean ± SD.

Results

Vip mRNA and Protein in tdTomato-Positive VIPcre Cells

We analyzed the specificity of red fluorescent protein-expressing cells (RFP+) for VIP-expressing cells in transgenic VIPcre/tdTomato mice by comparing RFP+ and the fluorescence derived from *Vip* RNA in situ probes via FISH and AB binding to the protein. For this quantification, fluorescent somata were counted in the barrel cortex in a layer-specific manner in 6 animals (3 sections per animal) for FISH and IHC, respectively.

At the RNA level, FISH using *Vip* probes labeled 2099.1 ± 113.2 cells/mm^3 cortex. 2372.9 ± 171.1 RFP+ cells/mm^3 cortex expressed tdTomato, of which 274.7 ± 168.5 cells/mm^3 cortex were not marked by *Vip* probes. Thus, 88.9% of all RFP+ cells co-localized with FISH-derived fluorescence. In layer I 64.1%, II/III 90.3%, IV 87.8%, Va 86.7%, Vb 88%, and VI 86% of RFP+ cells and FISH-derived fluorescent cells were co-localized. Only one soma in layer II/III showed fluorescence exclusively resulting from FISH (Fig. 1A–C and Fig. 2A–A″).

The analysis of VIP-IHC showed an even higher degree of co-localization: 2123.3 ± 337.4 cells/mm^3 cortex displayed RFP+, of which 2103.6 ± 332.9 cells/mm^3 cortex was labeled by αVIP AB IHC. Not a single cell was found, which showed immunofluorescence only. Thus, 99.1% of all RFP+ cells co-localized with αVIP AB. Subdivided into layers, 100% of RFP+ cells in layer I, 99% in layer II/III, 99.3% in layer IV, 100% in layer Va, 99.5% in layer Vb, and 98.4% in layer VI displayed AB-derived fluorescence (Fig. 1D–F). Furthermore, 2 different ABs from different sources yielded similar results (see Supplementary Fig. 4A,B). These results indicate that RFP+ is highly specific for VIP-expressing cells in VIPcre/tdTomato mice. In addition, tdTomato expression seems to be reliably strong in Cre-expressing neurons. This suggests that using transgenic VIPcre/tdTomato mice is a very sensitive method to identify VIP neurons.

VIP-Expressing Cells Are GABAergic and Do Not Express PV or SOM

According to most previous studies in rodents, cortical VIP-expressing interneurons are GABAergic (Bayraktar et al. 1997; Gonchar et al. 2007; Zeisel et al. 2015). Thus, we tested for the presence of *Gad1* RNA in RFP+ cells using FISH. 97.6% (2223.1 ± 283 of 2278.8 ± 284.2 cells/mm^3 cortex; n = 6 animals, 18 sections) of all VIP cells were also labeled using a *Gad1* probe (Fig. 2B). In contrast, FISH targeting RNA of the excitatory neuron marker *Vglut1* showed no co-localization at all (n = 3 animals, 9 sections; Fig. 2C), suggesting that most, if not all, VIP neurons are GABAergic.

Of all *Gad1*-expressing neurons (16869.1 ± 1792 cells/mm^3 cortex), a subpopulation of 13.2% also expressed VIP (2223.1 ± 283.0 cells/mm^3 cortex). This proportion varied across layers: in layer I 8.4% (72.9 ± 19.7 of 885.1 ± 219.2 cells/mm^3 cortex), in layer II/III 30.2% (1222 ± 140.6 of 4050.4 ± 473.2 cells/mm^3 cortex), in layer IV 13.0% (528.3 ± 104.3 of 4036.9 cells/mm^3 cortex), in layer Va

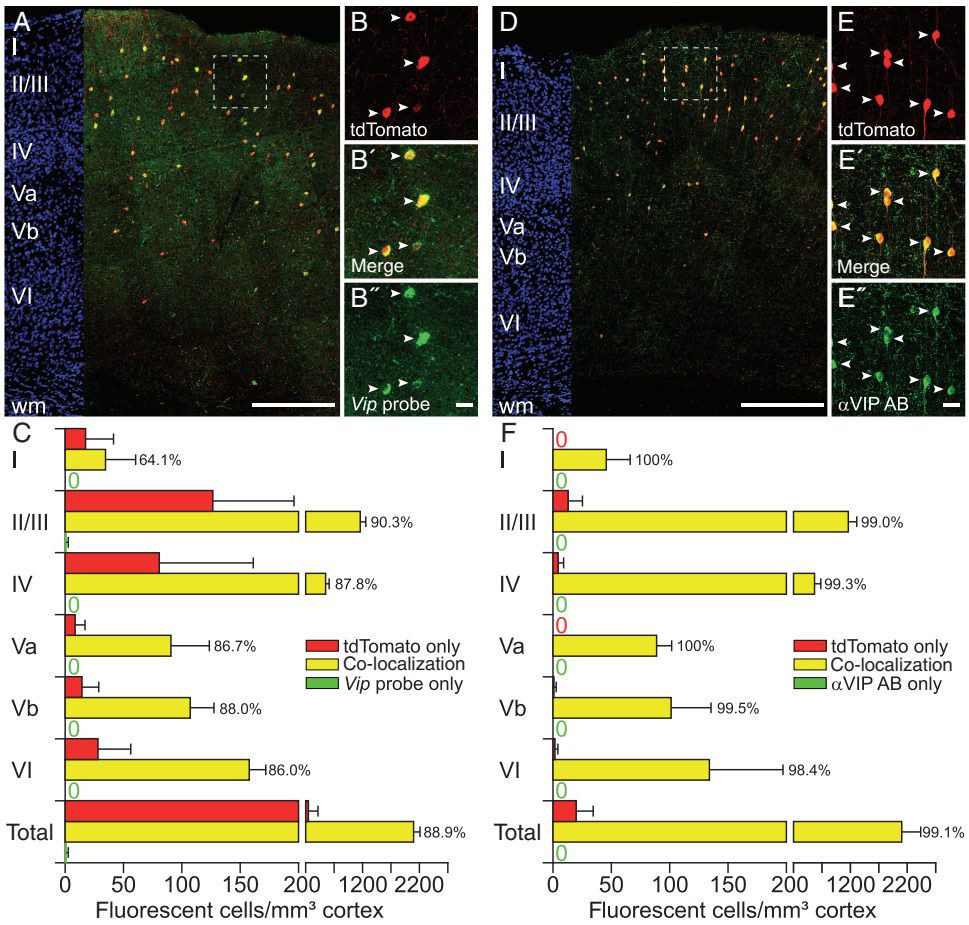

Figure 1. Sensitivity and specificity of Cre-driven fluorescence for VIP in VIPcre/tdTomato mice. (*A*) Projection view of a 50-µm thick coronal section treated with FISH utilizing an RNA probe specific for *Vip* through the barrel cortex of transgenic VIPcre/tdTomato mice. Layers were identified using DAPI staining (blue) and labeled with Roman numerals. The fluorescence of Cre-driven tdTomato expression is shown in red, and *Vip* probe-derived fluorescence in green. Any co-localization of fluorescence results in yellow (wm, white matter; scale bar = 250 µm). The white stippled outline marks the region of magnified views in (*B*–*B*″): Channels are shown separately as well as merged with tdTomato fluorescence at the top (*B*), *Vip* probe-derived fluorescence at the bottom (*B*″), and both signals overlaid in the middle (*B*′; same colors as in *A*; arrowheads point to co-localizations; scale bar = 20 µm). (*C*) Results of the analysis of population data for FISH (6 animals, 18 sections) are plotted as bar graphs in a layer-related manner, and summarized as cells/mm³ cortex. Red bars depict the number of cells that displayed tdTomato-derived fluorescence only, whereas yellow bars display the number of cells where fluorescence from tdTomato and FISH or IHC co-localizes. Cell bodies which were exclusively labeled by *Vip* probes are shown in green. A zero close to the *y*-axis indicates that no cells were found. Percentages close to co-localization bars display the fraction of tdTomato-positive cell bodies which co-localized with FISH (error bars = SD; roman numerals depict layers). Note that only a single cell body in layer II/III of the mouse barrel cortex exclusively showed *Vip* probe-derived fluorescence after FISH. (*D*–*E*″) Same as in (*A*), except that the section was treated with IHC using αVIP AB. (*F*) Results of the analysis of population data for IHC (6 animals, 18 sections) plotted as in (*C*). Co-localizations of Cre-driven fluorescence and fluorescence derived from FISH or IHC are consistently high across all layers of the barrel cortex in VIPcre/tdTomato mice. IHC yielded a larger fraction of co-localized cells than FISH (99.1% vs. 88.9%).

5.3% (91.9 ± 19.5 of 1773.5 ± 298.7 cells/mm³ cortex), in layer Vb 4.9% (128.6 ± 15.7 of 2686.5 ± 303.7 cells/mm^3 cortex), and in layer VI 5.0% (177.9 ± 51.8 of 3442.4 ± 332.9 cells/mm^3 cortex) of *Gad1*-expressing neurons also expressed VIP (see Supplementary Fig. 3).

As reported previously, the subpopulation of VIP-expressing interneurons does not overlap with other molecularly distinct major subpopulations, such as PV- or SOM-expressing interneurons (Rudy et al. 2011; Zeisel et al. 2015). To understand how distinct the population of VIP cells in the examined mouse model VIPcre/tdTomato is, we tested for co-localization of tdTomato and FISH with *Pvalb* ($n = 6$ animals, 18 sections; Fig. 2*D*) and *Sst* probes ($n = 6$ animals, 18 sections; Fig. 2*E*), respectively. We did not find a single overlap of these markers throughout the whole barrel cortex. The same results were obtained when using IHC with AB against PV ($n = 6$ animals, 16 sections; Supplementary Fig. 4*C*) and SOM ($n = 6$ animals, 18 sections; Supplementary Fig. 4*D*). Thus, these 3 protein markers distinguish the 3 major nonoverlapping subpopulations of GABAergic interneurons in VIPcre mice.

Distribution of Somata of VIP Neurons in the Barrel Cortex of VIPcre/tdTomato Mice

We quantified the distribution of VIP neurons in the barrel cortex of VIPcre/tdTomato mice in a layer-specific and a layer-independent (i.e., binned; see Materials and Methods and Supplementary Fig. 1 for details) manner ($n = 12$ animals, 150 sections; Fig. 3). Cell bodies were found throughout all layers of the barrel cortex with an overall number of 2226.4 ± 216.1 cells/mm^3 cortex. Nevertheless, the distribution of these cells was not homogeneous across layers. In layer I, the number of VIP cells (44.6 ± 40.5 cells/mm^3 cortex) was lowest compared with all other layers of the barrel cortex. Only 1.9% of all VIP cells were located in this

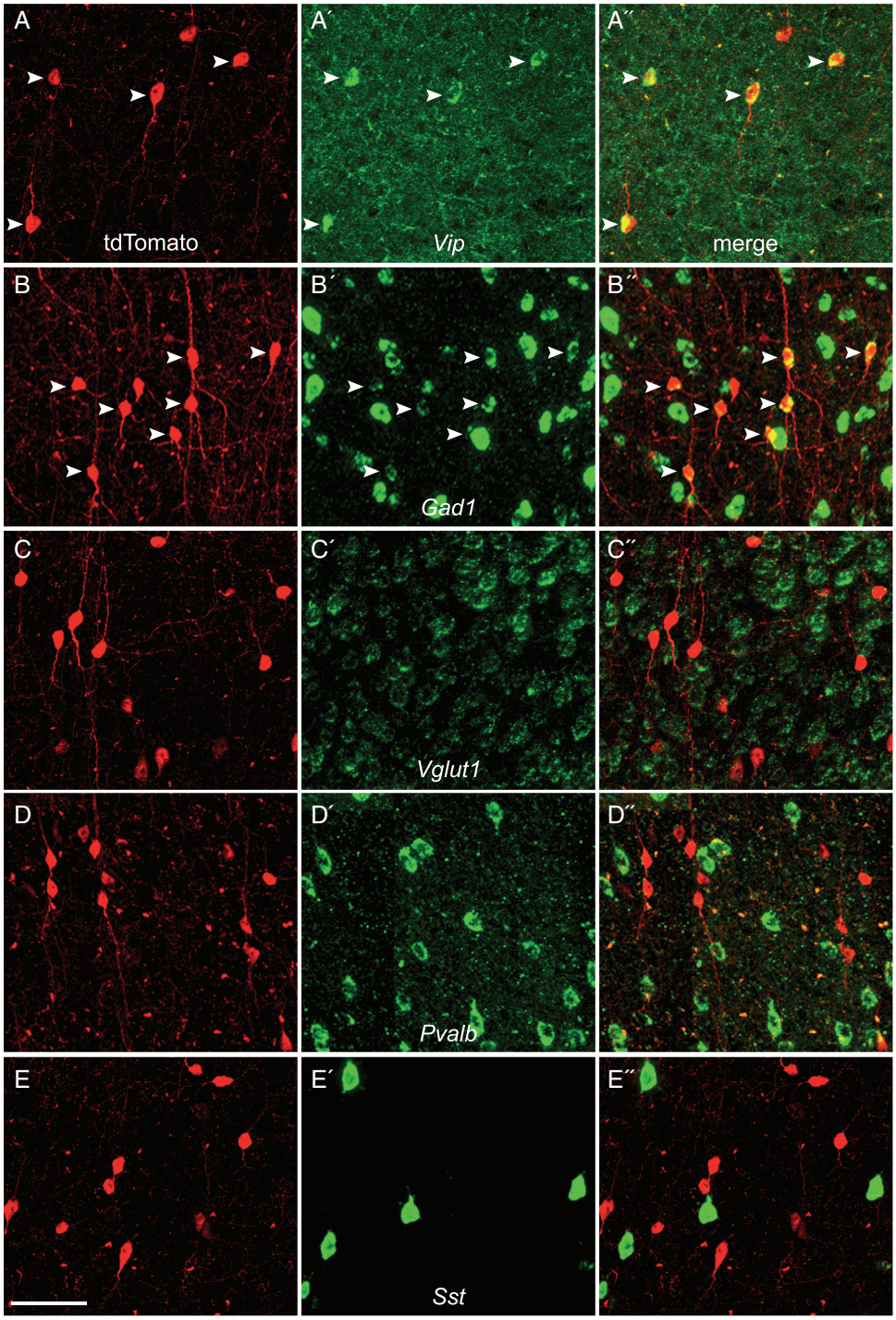

Figure 2. The GABAergic nature and distinction of VIP-expressing cells from other molecularly defined interneuron populations. Detailed views of layer II/III in individual 50-µm thick coronal sections through the barrel cortex in VIPcre/tdTomato mice are shown. Sections were treated with FISH using probes hybridizing with RNA of the genes *Vip* (*A*–*A*″), *Gad1* (*B*–*B*″), *Vglut1* (*C*–*C*″), *Pvalb* (*D*–*D*″), and *Sst* (*E*–*E*″). Vertical rows visualize (from left to right): Cre-driven tdTomato fluorescence in red (*A*–*E*), probe-derived fluorescence in green (*A*′–*E*′), and red and green channels merged, resulting in yellow co-localizations (*A*″–*E*″). Cell bodies that display both tdTomato and probe-derived fluorescence are marked by arrowheads (scale bar = 50 µm). Co-localizations are only seen using *Vip* and *Gad1* probes.

compartment. We observed the highest number of fluorescent cells in layer II/III: 1366.6 ± 285.8 cells/mm^3 cortex, which is 58.7% of all VIP cells in the barrel cortex. Layer IV was less populated (526.9 ± 168.95 cells/mm^3 cortex or 22.6%). The number of VIP cells further decreased in layer Va. Here, only 103.8 ± 46.5 cells/mm^3 cortex or 4.4% of all VIP cells were counted, followed by layer Vb with a similar count (119.0 ± 55.8 cells/mm^3 cortex or 5.0%). Layer VI also contained a comparatively small number of VIP cells (172.4 ± 76.4 cells/mm^3 cortex or 7.3%). The distribution of VIP cells was significantly different among all layers, except for layers Va and b (one-way ANOVA, $H = 859.838$, $P < 0.001$, post hoc Tukey analysis).

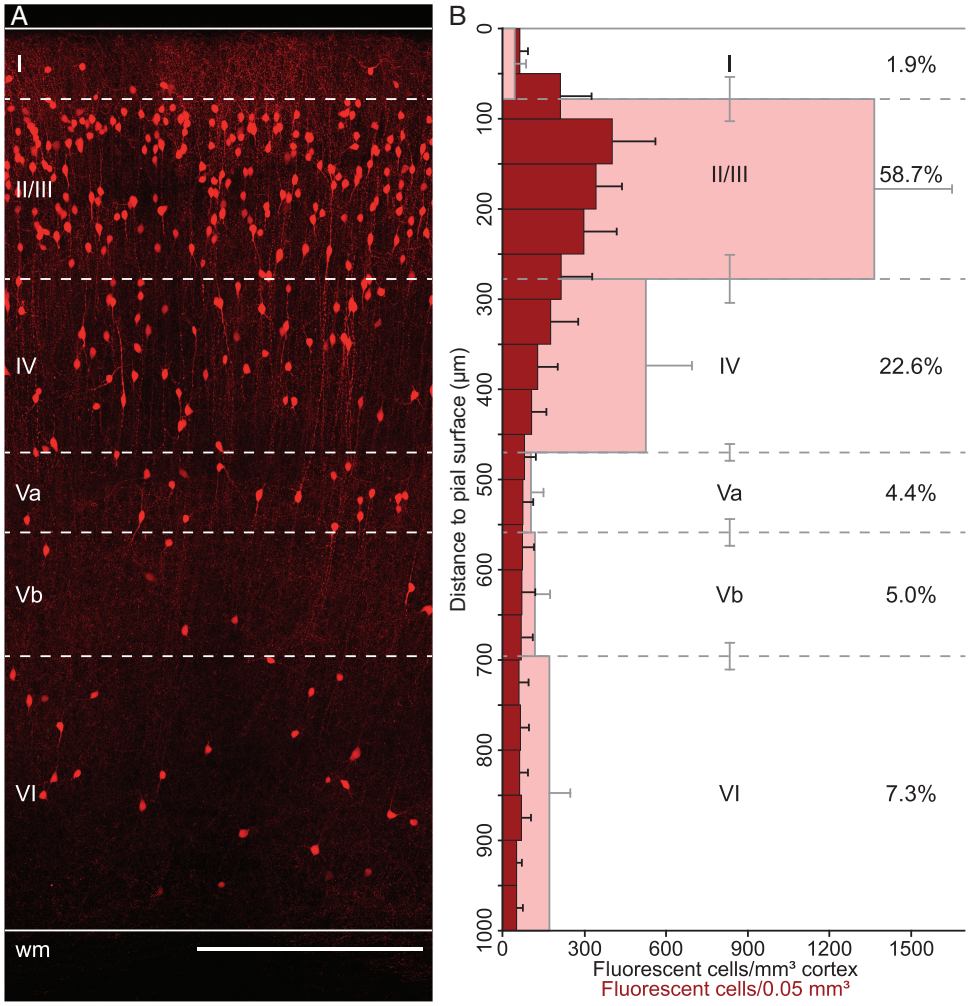

Figure 3. Distribution of fluorescent somata of VIP-expressing cells in the barrel cortex of VIPcre/tdTomato mice shows a clear peak in layer II/III. (*A*) Projection view of an image stack visualizing the native fluorescence in a 300-µm thick coronal section (as an exception to better illustrate the distribution of RFP+ cells) through the barrel cortex of a VIPcre/tdTomato mouse. wm, white matter. (*B*) Bar graphs depicting the population analysis of the density of RFP+ cells (*x*-axis) in a layer-dependent (light red in cells/mm^3 cortex; 12 animals, 150 sections) and layer-independent manner (dark red in cells/0.05 mm^3; 12 animals, 150 sections). The density in each layer is significantly different from all others (one-way ANOVA, $H = 983.520$, $P < 0.001$, post hoc Tukey analysis), except for layers Va and b. For the layer-independent analysis, somata were counted in 20 bins of 50 µm ranging from the pial surface (0 µm) to the white matter border (1000 µm; *y*-axis; dark red bar graph). The location of layer borders was determined by identifying layers in DAPI stainings of 150 sections from 12 animals. Layer thickness was measured perpendicular to the pial surface. The resulting mean is shown as dashed lines in *A* and *B* (roman numerals depict layers; error bars = SD; scale bar = 150 µm).

Even though the previous paragraph shows a realistic estimate of the count of VIP cells per layer in 1 mm^3 barrel cortex, differences in layer size prevent a direct comparison of cell densities between layers. To make this possible, we additionally calculated neuron densities per mm³ of the respective layer (cells/mm^3 layer X; see Materials and Methods and Supplementary Fig. 1 for details). In layer I, the density of VIP cells was lowest (500.1 ± 445.9 cells/mm^3 layer I). This increased to its maximum in layer II/III with 6432.4 ± 1163.5 cells/mm^3 layer II/III. In layer IV, we observed 2692.3 ± 786.7 cells/mm^3 layer IV. VIP cell density further decreased from layer Va (1175.7 ± 519.1 cells/mm^3 layer Va) to Vb (910.2 ± 425 cells/mm^3 layer Vb) and VI (617.6 ± 264 cells/mm^3 layer VI). The density of VIP cells was significantly different between all layers, except for layers Va and b (one-way ANOVA, $H = 663.938$, $P < 0.001$, post hoc Tukey analysis).

To analyze the distribution of VIP cells independent of the more subjective layer borders, we subdivided the distance between pial surface and white matter into 20 bins and determined the density of VIP cells in each (Fig. 3*B*). The density of VIP-expressing cells rapidly increased throughout the first 3 bins from the pial surface downward from 62.6 ± 30.0 to an overall maximum of 402.0 ± 158.4 cells/0.05 mm^3. From this peak, the density continuously decreased toward the white matter until it reached values below 100 cells/0.05 mm^3, that is, 79.9 ± 42.1 cells/0.05 mm^3, in the 10th bin. Further toward the white matter border, no major change in density was observed. The 20th bin contained the least amount of VIP cells with 50.9 ± 23.1 cells/0.05 mm^3. This pattern was reflected in a significance analysis (one-way ANOVA, $H = 983.520$, $P < 0.001$, post hoc Tukey analysis). The first 3 adjacent bins were significantly different from one another, indicating a rapid increase in cell density to its peak in upper layer II/III. The decrease, however, seemed to be roughly continuous, because the density in neighboring bins from the third on toward the last was not significantly different from each other. Furthermore, the respective number of VIP cells in bins 12 (layer Vb) to 20 (lower layer VI) was not significantly

different from the number of VIP cells in the first bin (layer I). This distribution corresponds well with most VIP cells being located in layers II/III and IV, whereas all other layers are less densely populated. Interestingly, the only distinct layer border reflected in the distribution pattern of VIP-expressing somata was between layers I and II/III. In addition, although the largest fraction of VIP cells is located in layer II/III (58.7%), a sizeable 41.9% of all VIP cells were found outside of this layer. As yet, these neurons have not been characterized to any significant extent.

Morphological Properties of Individual VIP Neurons

Because VIP neurons populate all layers of the barrel cortex and the spatial organization of these layers dictates the morphology of neurons, it is unlikely that this subgroup of GABAergic interneurons shows a similar morphology of somatodendritic and axonal arbors. In addition, different layers perform different functions (Harris and Shepherd 2015). To elucidate this in detail, we quantitatively analyzed the morphology of 18 individual VIP cells from all layers of the barrel cortex in VIPcre/tdTomato mice (layer I $n = 1$; layer II/III $n = 8$; layer IV $n = 3$; layer Va $n = 2$; layer Vb $n = 3$; layer VI $n = 1$; Figs 4–6; Supplementary Tables 1–3).

Somatodendritic Features

While VIP neurons were highly variable in most somatodendritic features, some were, however, invariant across the population. Somata of VIP neurons were predominantly elliptic (roundness = 0.62 ± 0.11; Supplementary Table 1) with a larger vertical diameter than a horizontal one (16.9 ± 2.3 and 11.0 ± 1.9 µm, respectively; Figs 4*B* and 5*B*; Supplementary Table 1). Somatodendritic configurations of VIP neurons were diverse and included [based on Bayraktar et al. (2000) and Ascoli et al. (2008)] 3 bipolar (Figs 4*Bc*,*Bd* and 5*Ba*), 6 modified bipolar (i.e., tripolar; Figs 4*Bb*, *Be* and 5*Bb*,*Bc*,*Bd*), 6 tufted (Fig. 5*Be*,*Bf*), 2 multipolar (Figs 4*Ba* and 5*Bg*), and 1 cell which did not fit into this nomenclature.

A superimposition of all reconstructed VIP cells showed that their dendrites were found in all layers of the barrel cortex, distributed as follows: 16.3% in layer I, 37.9% in layer II/III, 12.5% in layer IV, 9.1% in layer Va, 12.8% in layer Vb, 10.2% in layer VI, and 1.2% in the white matter (Fig. 6*A*).

Interestingly, more than half of all dendritic branches were found in supragranular layers I and II/III, although we analyzed an equal number of VIP neurons from the upper and deeper layers of the barrel cortex. Does this mean that dendritic trees of supragranular VIP neurons differ from those of the deeper layers? Indeed, we found significant differences in the vertical spread and the amount of extralaminar branches of dendrites: VIP neurons from layer II/III had a vertically more restricted dendritic tree compared with deeper layer VIP cells (310.2 ± 50.5 vs. 523.8 ± 170.9 µm, $U = 12.000$, $P = 0.024$; Fig. 6*A*,*C*). Additionally, VIP neurons from layer II/III extended fewer dendrites into the layers outside their home layer (location of soma) than VIP neurons from layers IV to VI (24.6 ± 12.1% vs. 61.9 ± 21%, $t = -4.141$, $P < 0.001$; Fig. 6*A*,*C*).

Axonal Features

The morphology of axonal trees of VIP neurons was also highly variable among individual VIP neurons. Some features, however, remained consistent. In only 2 of 18 VIP neurons did the axon emanate from the soma itself (Fig. 5*Bg*). In 16 of the neurons, the axon originated from a first-, second-, or even third-order dendrite directed toward the white matter (Figs 4*B* and 5*B*). As a population, axonal ramifications were found in all layers of the barrel cortex (Fig. 6*B*). We analyzed several axonal features such as total length (8075.6 ± 3266.9 µm), number of nodes (116.3 ± 54.6), and horizontal (381.8 ± 205.2 µm) and vertical (690.5 ± 281.3 µm) spread. As with dendritic features, we compared axonal properties of layer II/III VIP neurons with those of layers IV–VI. Interestingly, only the vertical spread of axonal trees was significantly different: Layer II/III VIP neurons extended their axons across all layers of the barrel cortex, whereas layer IV–VI VIP neurons had more restricted axonal trees (vertical spread of 965.9 ± 95 vs. 499.7 ± 142 µm, $t = 7.380$, $P < 0.001$; Fig. 6*B*,*C*).

We also determined the number of axonal boutons of VIP neurons (2438.7 ± 1325.2; 29.3 ± 5.7 boutons per 100 µm axon) as well as their precise localization. In correlated light and electron microscopic studies, these structures were previously described as sites of presynaptic specializations (Staiger et al. 2004b; David et al. 2007). Thus, we analyzed their distribution profile across the barrel cortex. For layer II/III VIP neurons, most of the axonal boutons were found in 2 hot spots corresponding to layers II/III (42.8%) and Va (22.3%). The remainder was distributed as follows: 2.4% in layer I, 13.3% in layer IV, 13% in layer Vb, and 6% in layer VI. In contrast, VIP neurons located in deeper layers IV–VI showed a different distribution of axonal boutons. Most of these were found in layers Vb (43.9%) and VI (35.8%). Interestingly, no boutons were found in layer I and only few in layers II/III (0.4%), IV (10.6%), and Va (10.1%; Fig. 6*B*).

In summary, VIP neurons with their somata in layer II/III had slender axonal trees spreading across all layers of the barrel cortex with preferences for layers II/III and Va. VIP neurons with somata in deeper layers, however, showed more locally restricted axonal trees with preferences for layers Vb and VI.

Essentially, the layer targeting of both dendritic and axonal trees was heavily dependent on the location of the soma of VIP-expressing neurons in the barrel cortex of mice (Fig. 6; Supplementary Tables 1–3). This suggests that the 2 populations (layer II/III vs. layer IV–VI) possess distinct input and output domains.

Electrophysiological Profile of VIP Neurons

We determined membrane properties of 69 VIP neurons from all layers of the barrel cortex (layer I $n = 1$; layer II/III $n = 34$; layer IV $n = 7$; layer Va $n = 7$; layer Vb $n = 9$; layer VI $n = 11$; Figs 4*C*, 5*C*, and 7; Supplementary Tables 4 and 5). Since we observed morphological differences which were dependent on the location of their somata, we asked whether such differences also exist on the level of electrophysiology. Thus, we compared electrophysiological data of 34 neurons from layer II/III with 34 neurons from layers IV to VI (Fig. 7; Supplementary Tables 4 and 5). No significant differences were found in most of the basic properties such as in input resistance (population average of 404.7 ± 212.8 MΩ), sag index (11.2 ± 6.8%), τ (21.4 ± 7.6 ms), rheobase (51.9 ± 33.9 pA), firing threshold (−38.2 ± 3.1 mV), amplitude of action potentials (65.1 ± 9.1 mV), rise time of action potentials (0.75 ± 0.16 ms), half width of action potentials (0.89 ± 0.21 ms), slope of action potentials (118.3 ± 34.5 V/s), or drop of amplitude of the first to the second action potential in a spike train (−5.2 ± 4.0 mV; see Supplementary Tables 3 and 4; Fig. 7; see Figs 4*C* and 5*C* for individual examples). VIP neurons showed a great variability in timing and composition of AHP: faster (1.2 ± 0.42 ms; fAHP) and slower peaking AHPs (31.7 ± 20 ms; medium AHP; mAHP). fAHP and mAHP occurred sequentially or individually. Two passive membrane properties, however, were significantly different in the 2 VIP neuron populations: VIP neurons from layer II/III were

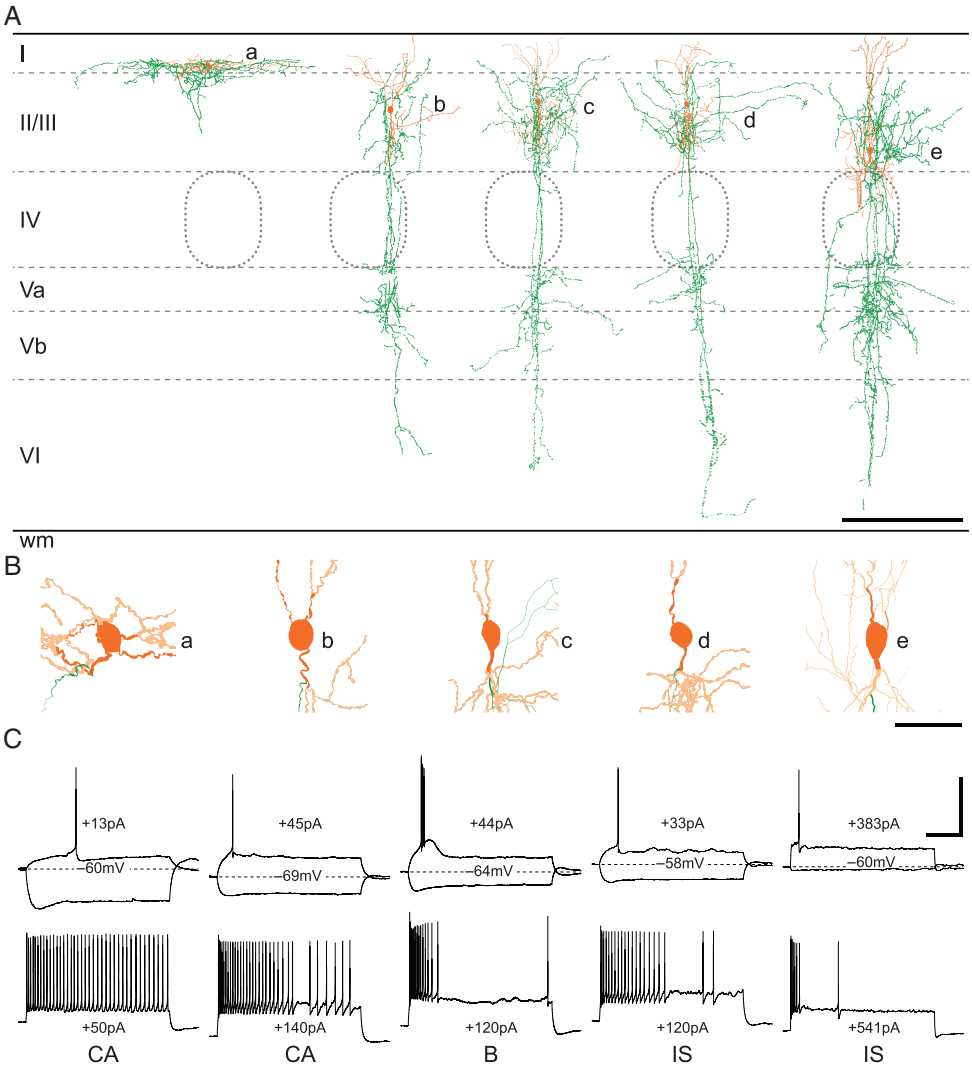

Figure 4. Morphology and electrophysiology of VIP-expressing interneurons from layers I–II/III in the barrel cortex of VIPcre/tdTomato mice. (*A*) The reconstructed morphology of 5 individual VIP neurons is shown in a schematized barrel cortex. It is obvious that layer II/III VIP neurons (b–e) are similar to each other but very different from a layer I (a) neuron. Somata and dendrites are colored orange, and axonal processes green. In layer IV, the position of the home barrel for each neuron is depicted as dotted outlines, whereas dashed horizontal lines show layer borders. Individual neurons are labeled with lower case letters (layer borders as in Fig. 3; roman numerals indicate layers; wm, white matter; scale bar = 250 µm). (*B*) Magnified views of somatodendritic configurations for each neuron show multipolar (a), bipolar (c,d), and modified bipolar (b,e) patterns. Somata and first-order segments of the primary dendrites are colored in dark orange, higher order branches in a light orange, and axon in green (scale bar = 25 µm). (*C*) Electrophysiological recordings reveal a large diversity of membrane properties at rheobase (values in pA; upper traces) and in response to a hyperpolarizing current pulse of −50 pA. Dashed horizontal lines indicate the resting membrane potential. Action potential firing patterns (lower traces) show no correlation with the morphological properties. Note that the recordings for the neuron from layer I do not match the reconstructed cell. Abbreviations name the firing pattern after the Petilla convention (Ascoli et al. 2008; CA, continuous adapting; IS, irregular spiking; B, bursting; scale bars = 50 mV/250 ms).

more depolarized in their resting state than those found in deeper layers (somatic resting membrane potential of −66.3 ± 4.8 vs. −70.1 ± 5.4 mV; $t = 3.207$; $P = 0.001$). Furthermore, there was less fast rectification in upper layer VIP neurons (RI of 4.0 ± 3.1% vs. 9.7 ± 5.8%; $U = 216.000$; $P < 0.001$; see Materials and Methods for details). In addition, the amplitudes of fAHP and mAHP were smaller in VIP neurons from layer II/III compared with those of layers IV–VI (fAHP: −8.6 ± 3.1 vs. −11.2 ± 3.4 mV; $t = 2.930$; $P = 0.005$; mAHP: −12.1 ± 2.3 vs. −13.5 ± 2.2 mV; $U = 229.000$; $P = 0.032$; Fig. 7; Supplementary Tables 4 and 5).

VIP neurons also showed great variability in firing patterns. They were never fast-spiking, but, following the Petilla convention (Ascoli et al. 2008), showed the following firing patterns: continuous adapting (75.4%), irregular spiking (14.5%), bursting (5.8%), or high threshold bursting nonadapting (4.3%; see Figs 4C and 5C for examples). In layer II/III, 67.6% of all VIP neurons were continuous adapting, 14.7% irregular spiking, 11.8% bursting, and 5.9% high threshold bursting nonadapting. In layers IV–VI, 82.4% of all VIP neurons were continuous adapting, 14.7% irregular spiking, and 2.9% high threshold bursting nonadapting. Bursting VIP neurons were exclusively observed in layer II/III.

Discussion

In this study, we show that *Vip-ires-cre* mice drive fluorophore expression in the entire population of VIP-immunoreactive interneurons in the barrel cortex of mice. These neurons also express Gad1, but not vGluT1, PV, or SOM, in all layers of the barrel cortex. Thus, we validate that *Vip-ires-cre* mice are a highly specific and sensitive model system for studying VIP-expressing

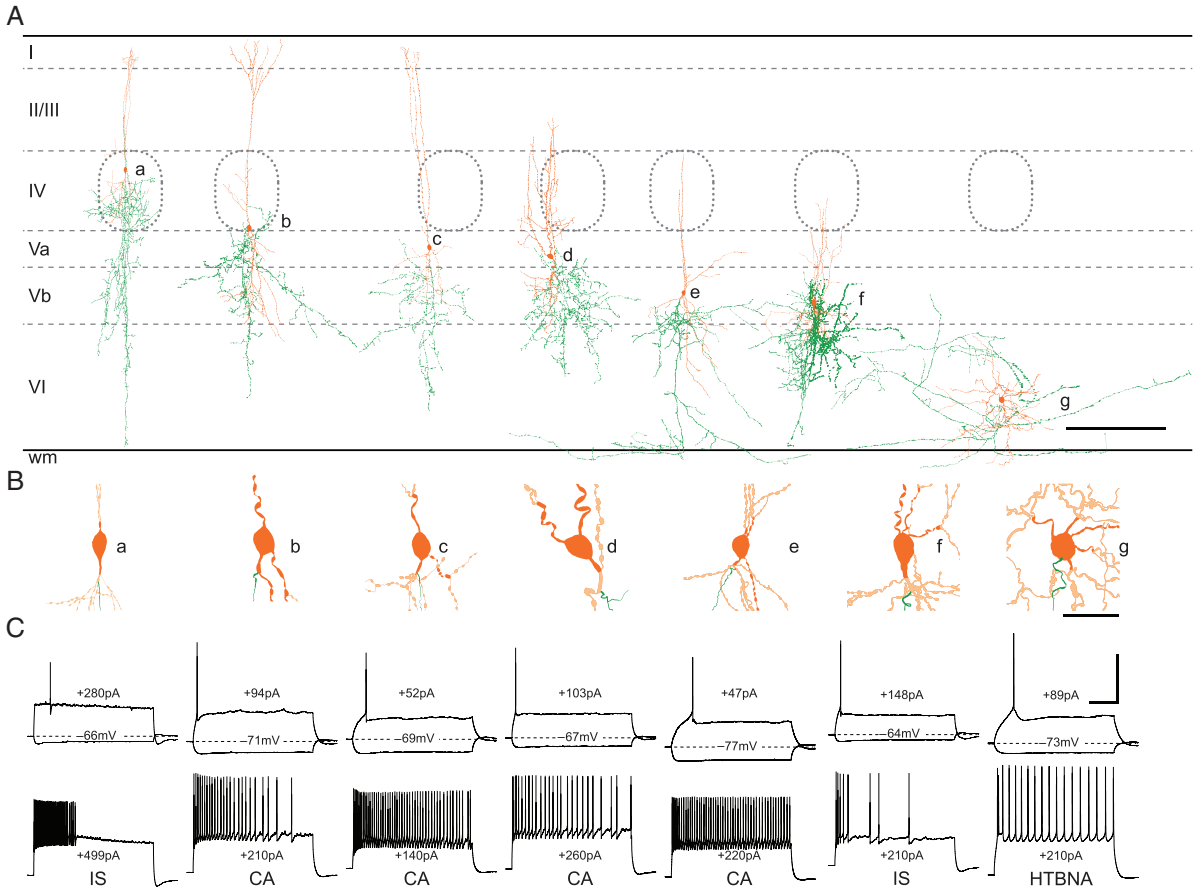

Figure 5. Morphology and electrophysiology of VIP-expressing interneurons from layers IV–VI in the barrel cortex of VIPcre/tdTomato mice. (*A*) The reconstructed morphology of 7 individual VIP neurons is shown in a schematized barrel cortex. Somata and dendrites are colored orange, and axonal processes green. In layer IV, the position of the home barrel for each neuron is depicted as dotted outlines, whereas dashed horizontal lines show layer borders. Individual neurons are labeled with lower case letters (layer borders as in Fig. 3; roman numerals indicate layers; wm, white matter; scale bar = 250 µm). (*B*) Magnified views of somatodendritic configurations for each neuron show differences between bipolar (a), (bi-) tufted (e,f), modified bipolar (b–d), and multipolar (g) patterns. Somata and first-order segments of the primary dendrites are colored in dark orange, higher order branches in a light orange, and axon in green (scale bar = 25 µm). (*C*) Electrophysiological recordings reveal a large diversity of membrane properties at rheobase (values in pA; upper traces) and in response to a hyperpolarizing current pulse of –50 pA. Dashed horizontal lines indicate the resting membrane potential. Action potential firing patterns (lower traces) show no correlation with the morphological properties. Abbreviations name the firing pattern after the Petilla convention (Ascoli et al. 2008; CA, continuous adapting; IS, irregular spiking; HTBNA , high threshold bursting nonadapting; scale bars = 50 mV/250 ms).

interneurons (Taniguchi et al. 2011). This model enabled us to describe the distribution, morphology, and electrophysiology of VIP neurons in the barrel cortex of mice. Our main findings include the fact that besides layer II/III-located bipolar/bitufted cells, there is a significantly different population of VIP neurons in layers IV–VI. This raises the question of whether the recently described function of VIP neurons as integrators of long-distance inputs into local cortical circuitry is dependent on both populations or whether they might contribute to different, but as yet unexplored functions (Lee et al. 2013; Pi et al. 2013; Fu et al. 2014; Zhang et al. 2014).

Validation of the Cre-Driver Line as a Suitable Model System for Studying VIP Neurons

Specific targeting of VIP-expressing interneurons was very difficult in the past when these neurons were identified in nontransgenic approaches (Bayraktar et al. 2000; Cauli et al. 2000; Karagiannis et al. 2009). However, advances in the generation of transgenic mouse lines made VIP neurons more accessible. Early BAC-transgenic mouse lines had the disadvantages of either labeling VIP neurons as part of a larger population of neurons (ChAT-eGFP, von Engelhardt et al. 2007; GAD65-eGFP or G30, Xu and Callaway 2009; CR-eGFP, Caputi et al. 2009; Miyoshi et al. 2010) or being too unreliable in transgene expression (VIP-eGFP, own unpublished observation). Recently, a Cre-driver line for VIP was introduced, which promises a high degree of specificity and sensitivity (Taniguchi et al. 2011), but still required thorough characterization since previous studies were based on a low number of cells and confined to supragranular layers of the barrel cortex.

We used FISH and IHC to label VIP neurons in conjunction with Cre-driven tdTomato fluorescence. The almost perfect co-localization of fluorescence across all layers of the barrel cortex demonstrates the extensive sensitivity and specificity of this mouse line. In addition, FISH only labeled 89% of all tdTomato-expressing cells, whereas IHC labeled 99%. Thus, VIPcre/tdTomato mice seem to display VIP neurons more sensitive and specific than FISH or IHC could detect. We could also show that VIP neurons do not co-localize with the excitatory marker *vGluT1*, but indeed express *Gad1* in the barrel cortex of mice, ruling out the possibility that at least some VIP neurons are excitatory

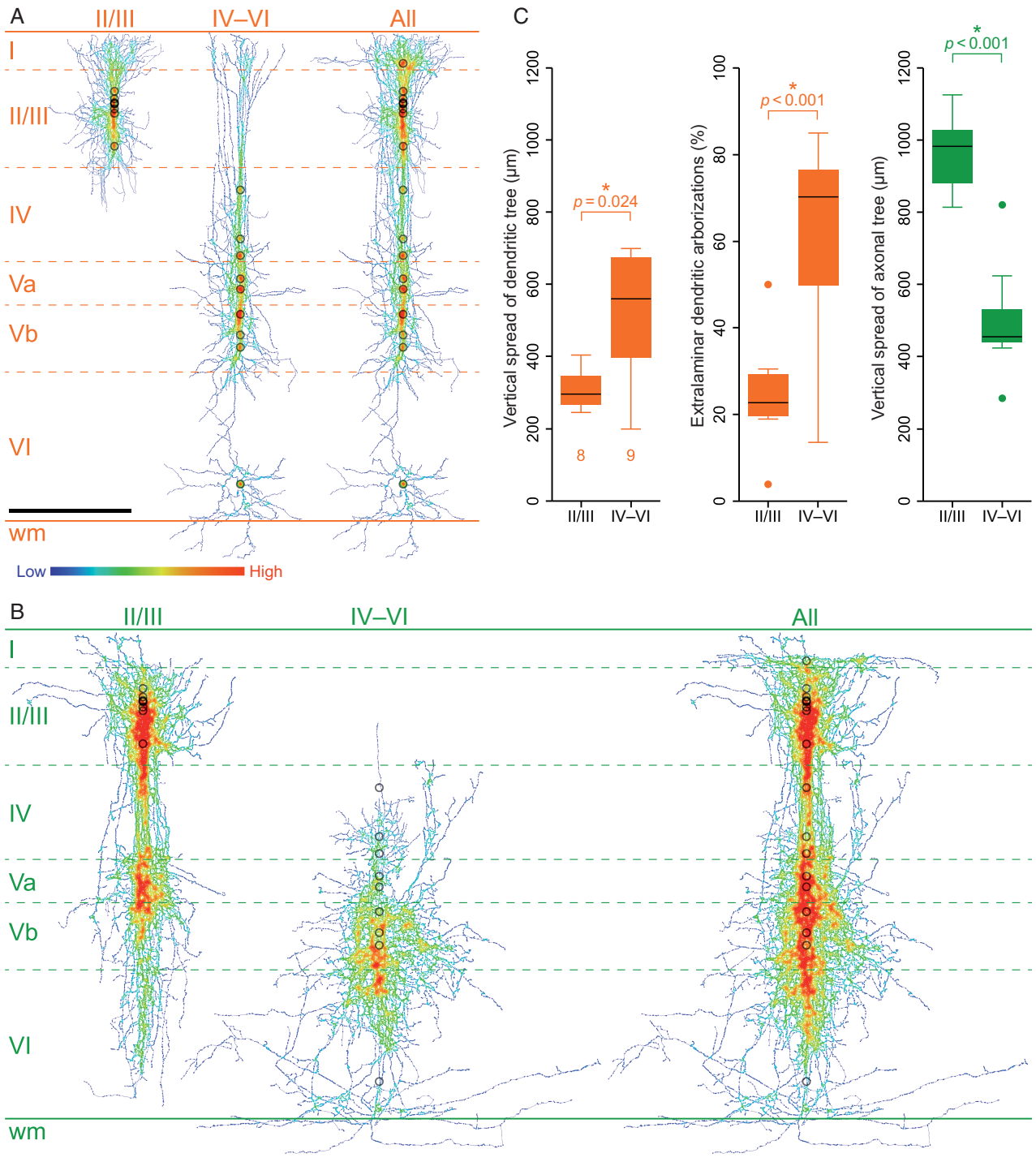

Figure 6. Somatodendritic and axonal morphology of VIP neurons from layer II/III is different from VIP neurons from layers IV to VI. (*A*) Reconstructions of the somatodendritic morphology of superimposed layer II/III VIP neurons show the restriction of the input compartment to layers I–III, whereas layer IV–VI neurons spread their dendritic arbors across all layers. (*B*) Axonal arbors show the opposite structural organization: Layer II/III axons spread across all layers of the barrel cortex, whereas layer IV–VI VIP neurons restrict their axon to the same layer compartment. The density of structures is visualized as heat maps ranging from red (most dense) to blue (least dense). Positions of somata are vertically aligned and marked as gray open circles. Eight VIP neurons from layer II/III are superimposed on the left, 9 from layers IV to VI in the middle, and all of these neurons merged including 1 layer I neuron are shown on the right in (*A* and *B*) (roman numerals depict layers; scale bar = 250 µm). (*C*) Box plots depicting significantly different features of dendrites and axons between the 2 tested groups (vertical spread of dendritic trees: 310.2 ± 50.5 vs. 523.8 ± 170.9 µm, $U = 12.000$, $P = 0.024$; amount of extralaminar dendritic arborizations: 24.6 ± 12.1% vs. 61.9 ± 21%, $t = -4.141$, $P < 0.001$; vertical spread of axonal trees: 965.9 ± 95 vs. 499.7 ± 142 µm, $t = 7.380$, $P < 0.001$; see Supplementary Tables 1–3 for all tested parameters).

(von Engelhardt et al. 2007; Wouterlood et al. 2008). The percentage of VIP neurons of the GABAergic neuron population was 13.2% and varied across layers. The highest percentage was observed in layer II/III, where 30.2% of all GABAergic neurons express VIP. In addition, VIP neurons never expressed molecular markers of other major populations of GABAergic neurons such

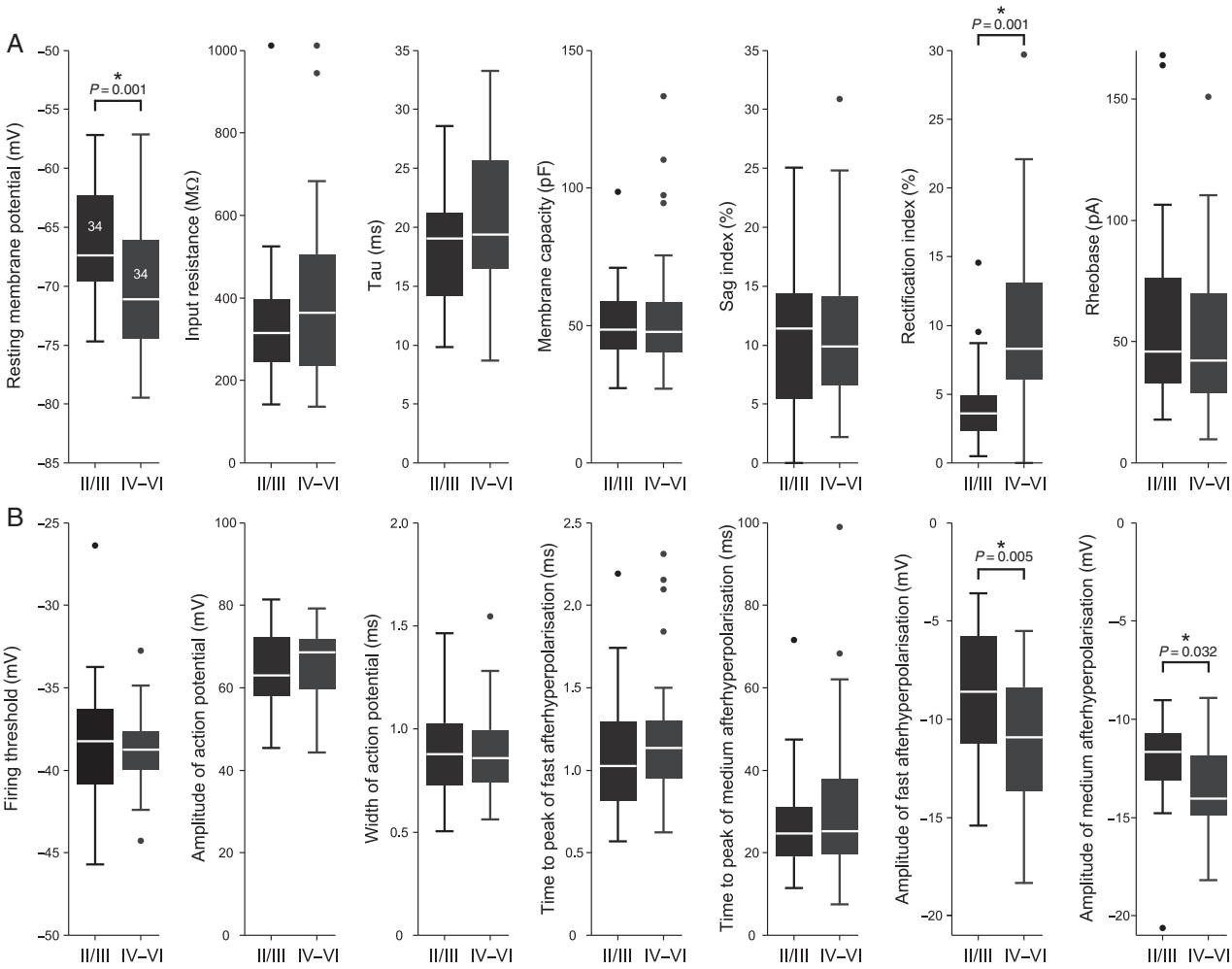

Figure 7. Comparison of electrophysiological properties of VIP neurons from layer II/III to neurons from layers IV to VI. (*A*) Box plots describing various passive and membrane properties of 68 VIP neurons separated into neurons from layer II/III ($n = 34$) and layers IV–VI ($n = 34$). (*B*) Box plots showing various active membrane properties as in (*A*). Significant differences were found in the resting membrane potential (−66.3 ± 4.8 vs. −70.1 ± 5.4 mV, $t = 3.207$, $P = 0.00102$), the amount of fast rectification (4.01 ± 3.1% vs. 9.7 ± 5.8%, $U = 216.000$, $P < 0.001$), and the amplitudes of fAHP and mAHP (fAHP: −8.6 ± 3.1 vs. −11.2 ± 3.4 mV, $t = 2.930$, $P = 0.005$; mAHP: −12.1 ± 2.3 vs. −13.5 ± 2.2 mV, $U = 229.000$, $P = 0.032$; see Supplementary Tables 3 and 4 for more details).

as SOM or PV. These findings confirm and greatly extend previous data, thus enabling us to selectively and specifically study the properties of VIP neurons (Rudy et al. 2011; Lee et al. 2013; Pfeffer et al. 2013; Pi et al. 2013; Fu et al. 2014; Karnani et al. 2014).

VIP Neurons Show a Broad Spectrum of Morphological and Electrophysiological Properties

Our detailed analysis of the distribution of VIP neurons across the barrel cortex of mice revealed that VIP neurons are found in all layers. While the majority is found in layer II/III (~60%), thus confirming earlier studies (Taniguchi et al. 2011), a large fraction (~40%) is also found outside of this upper layer.

In this study, we show reconstructions of individual VIP neurons from all layers of the barrel cortex despite a low recovery rate of approximately 10%, which could be due to their small soma size. VIP neurons from the barrel cortex of mice show a much greater variability in morphological properties than the classical bipolar neuron described in the early literature (Morrison et al. 1984). Somatodendritic configurations are not restricted to bipolar, but also include tufted and even multipolar appearances.

Interestingly, the majority of axons of VIP neurons emanated not directly from the cell body, but from a dendrite extending toward the white matter. It has been shown that this structural organization has an impact on the efficacy of postsynaptic currents in different parts of the dendritic tree: Postsynaptic currents that are evoked in the dendritic tree carrying the axon have a greater impact on the generation of action potentials than those which have to pass the soma before arriving at the axon initial segment (Häusser et al. 1995; Thome et al. 2014). Since the axon of VIP neurons primarily originates at a dendrite oriented toward the white matter, the input to these dendrites might have more impact on spike generation than input to dendrites oriented toward the pial surface. Previous studies identified several sources of input onto VIP neurons: local pyramidal cells (Porter et al. 1998), thalamic fibers from the ventroposteromedial nucleus (Staiger et al. 1996), the basal forebrain (Fu et al. 2014), and cross-areal fibers (Lee et al. 2013). So far, little is known about the precise origin of synapses on the dendritic trees of VIP neurons. Nevertheless, axonal fibers from the motor cortex are considered to preferentially terminate in layer I. Some VIP neurons extend dendrites, which do not carry an axon into this layer. Thus, input from

the motor cortex might not be as influential in driving VIP neurons as yet unidentified input to axon-carrying dendrites.

Membrane properties were similar, but not the same as was previously reported. We confirm that the most abundant firing pattern is continuous adapting (~75%) as Karagiannis et al. (2009) showed. Their study also identified bursting VIP neurons which we found exclusively in layer II/III. In addition, we also observed irregular spiking and high threshold bursting nonadapting VIP neurons. Most membrane properties, however, were similar to those reported in rats (Porter et al. 1998; Karagiannis et al. 2009). Dissimilarities to prior reports from rats can be explained by methodological differences, such as identification of VIP neurons, number of cells analyzed, age of the animals, or analyzing techniques, and do not necessarily reflect interspecies differences.

Almost 60% of VIP neurons are located in layer II/III. Their appearance seems to be more homogeneous than that of approximately 40% of VIP neurons from other layers of the barrel cortex. Thus, we pooled data from VIP neurons from layer II/III and layers IV–VI, and compared these subgroups statistically: The morphology of layer II/III VIP neurons suggests that their dendritic tree is confined to layers I and II/III, whereas their axon is found across all layers of the barrel cortex. In contrast, dendrites of VIP neurons from layers IV to VI are found in all layers of the barrel cortex, whereas their axon is virtually confined to layers V and VI. Interestingly, none of the other morphological parameters tested were significantly different. This suggests that the structural organization or blueprint of dendritic and axonal trees is similar in every VIP neuron, whereas the distribution of these fibers is dependent on the location of the soma.

We also found differences in electrophysiological properties of layer II/III VIP neurons compared with the deeper layer neurons. VIP neurons from layer IV–VI are more hyperpolarized than those of layers II/III, which suggests that the latter are more easily excited. Furthermore, the amount of fast inward rectification is greater in the deeper layer VIP neurons. Fast inward rectification is a mechanism to stabilize resting membrane potentials in more hyperpolarized states. Thus, it is not surprising that VIP neurons in the deeper layers display greater fast inward rectification, while their resting membrane potential is more hyperpolarized. Interestingly, VIP neurons from layer IV to VI also show AHPs with larger amplitudes.

Functional Implications

The morphology of the dendritic trees of VIP neurons suggests that these neurons, as a population, are capable of receiving input from all layers of the barrel cortex. However, the input domain of layer II/III VIP neurons is found in layers I and II/III, whereas VIP neurons from layers IV to VI cover more possible layers of input. Some of these neurons reach into layer I, whereas others stay within layers IV to VI. This suggests that these neurons might integrate other sources of input than the much more homogeneous VIP neurons in layer II/III. The population of VIP neurons sends axonal branches across every layer of the barrel cortex. Layer II/III VIP neurons, however, preferentially target layers II/III and Va. In contrast, VIP neurons in layers IV–VI preferentially target layers Vb and VI. This supports the presumption of VIP neurons being differentially integrated in as yet unidentified cortical circuits.

Previous studies have shown that layer II/III VIP neurons are involved in a disinhibitory circuit motif that operates under behaviorally relevant conditions. In this scenario, VIP neurons receive input from axons originating in other cortical areas and the basal forebrain (Lee et al. 2013; Fu et al. 2014). These inputs allow them to integrate widespread cortical motor commands and sensory information with a saliency signal coming from the basal forebrain, which is considered to be cholinergic (Muñoz and Rudy 2014; Poorthuis et al. 2014). VIP neurons respond strongly to cholinergic agonists (Porter et al. 1999) and this activation, together with the intracortical drive, leads to an inhibition of their target neurons, which often are other inhibitory neurons, for example, SOM-expressing interneurons which themselves inhibit pyramidal cells. Thus, an activation of VIP neurons leads to an inhibition of SOM and a subpopulation of PV neurons. This releases pyramidal cells from inhibition and results in an increased gain of function in sensory information processing in the cortex (Staiger et al. 2004b; David et al. 2007; Lee et al. 2013; Pfeffer et al. 2013; Pi et al. 2013; Fu et al. 2014). We found morphological properties of VIP neurons in the barrel cortex, which could fit this circuit motif: The largest fraction of VIP neurons (~60%) populates layer II/III. These neurons reliably extend their dendritic trees across layers I–III, which is the layer where fibers from other cortical areas terminate (Lee et al. 2013). Most of the axonal boutons of VIP neurons are found in layers II/III and, interestingly, Va/b. Previous reports have shown that a substantial fraction of inhibitory interneurons in these 2 layers expresses PV and SOM (Gonchar et al. 2007; Xu et al. 2010). Thus, axonal trees of VIP neurons are well capable of targeting these aforementioned inhibitory neuronal populations.

An approximately 40% of VIP neurons outside of layer II/III seem to have different domains of input and output. Whether these neurons also partake in the aforementioned disinhibitory circuit motif or integrate into other cortical circuits needs further inquiry. For this and many other questions involving VIP neurons, *Vip-ires-cre* mice are a highly reliable research tool.

Supplementary Material

Supplementary material can be found at: http://www.cercor.oxfordjournals.org/.

Funding

This work was supported by the Deutsche Forschungsgemeinschaft (STA 431/8-1 and 10-1) and by the CRC 889 (Cellular mechanisms of sensory information processing; TP C07 to J.F.S.). Funding to pay the Open Access publication charges for this article was provided by the DFG via the CRC 889.

Notes

We thank Anna Dudek for help with the manuscript, Patricia Sprysch, Sandra Heinzl, and Anna Dudek for excellent technical assistance, and Anette Mertens and Adrian Villalobos for their help with the reconstructions. *Conflict of Interest*: None declared.

References

Ascoli GA, Alonso-Nanclares L, Anderson SA, Barrionuevo G, Benavides-Piccione R, Burkhalter A, Buzsaki G, Cauli B, Defelipe J, Fairen A, et al. 2008. Petilla terminology: nomenclature of features of GABAergic interneurons of the cerebral cortex. Nat Rev Neurosci. 9:557–568.

Bayraktar T, Staiger JF, Acsady L, Cozzari C, Freund TF, Zilles K. 1997. Co-localization of vasoactive intestinal polypeptide, gamma-aminobutyric acid and choline acetyltransferase in neocortical interneurons of the adult rat. Brain Res. 757:209–217.

Bayraktar T, Welker E, Freund TF, Zilles K, Staiger JF. 2000. Neurons immunoreactive for vasoactive intestinal polypeptide in the rat primary somatosensory cortex: morphology and spatial relationship to barrel-related columns. J Comp Neurol. 420:291–304.

Caputi A, Rozov A, Blatow M, Monyer H. 2009. Two calretinin-positive GABAergic cell types in layer 2/3 of the mouse neocortex provide different forms of inhibition. Cereb Cortex. 19:1345–1359.

Cauli B, Porter JT, Tsuzuki K, Lambolez B, Rossier J, Quenet B, Audinat E. 2000. Classification of fusiform neocortical interneurons based on unsupervised clustering. Proc Natl Acad Sci USA. 97:6144–6149.

Cauli B, Tong XK, Rancillac A, Serluca N, Lambolez B, Rossier J, Hamel E. 2004. Cortical GABA interneurons in neurovascular coupling: relays for subcortical vasoactive pathways. J Neurosci. 24:8940–8949.

David C, Schleicher A, Zuschratter W, Staiger JF. 2007. The innervation of parvalbumin-containing interneurons by VIP-immunopositive interneurons in the primary somatosensory cortex of the adult rat. Eur J Neurosci. 25:2329–2340.

DeFelipe J, Lopez-Cruz PL, Benavides-Piccione R, Bielza C, Larranaga P, Anderson S, Burkhalter A, Cauli B, Fairen A, Feldmeyer D, et al. 2013. New insights into the classification and nomenclature of cortical GABAergic interneurons. Nat Rev Neurosci. 14:202–216.

Fu Y, Tucciarone JM, Espinosa JS, Sheng N, Darcy DP, Nicoll RA, Huang ZJ, Stryker MP. 2014. A cortical circuit for gain control by behavioral state. Cell. 156:1139–1152.

Gonchar Y, Wang Q, Burkhalter A. 2007. Multiple distinct subtypes of GABAergic neurons in mouse visual cortex identified by triple immunostaining. Front Neuroanat. 1:3.

Haider B, McCormick DA. 2009. Rapid neocortical dynamics: cellular and network mechanisms. Neuron. 62:171–189.

Harris KD, Shepherd GM. 2015. The neocortical circuit: themes and variations. Nat Neurosci. 18:170–181.

Häusser M, Stuart G, Racca C, Sakmann B. 1995. Axonal initiation and active dendritic propagation of action potentials in substantia nigra neurons. Neuron. 15:637–647.

Karagiannis A, Gallopin T, David C, Battaglia D, Geoffroy H, Rossier J, Hillman EM, Staiger JF, Cauli B. 2009. Classification of NPY-expressing neocortical interneurons. J Neurosci. 29: 3642–3659.

Karnani MM, Agetsuma M, Yuste R. 2014. A blanket of inhibition: functional inferences from dense inhibitory connectivity. Curr Opin Neurobiol. 26:96–102.

Klausberger T, Somogyi P. 2008. Neuronal diversity and temporal dynamics: the unity of hippocampal circuit operations. Science. 321:53–57.

Lee S, Hjerling-Leffler J, Zagha E, Fishell G, Rudy B. 2010. The largest group of superficial neocortical GABAergic interneurons expresses ionotropic serotonin receptors. J Neurosci. 30:16796–16808.

Lee S, Kruglikov I, Huang ZJ, Fishell G, Rudy B. 2013. A disinhibitory circuit mediates motor integration in the somatosensory cortex. Nat Neurosci. 16:1662–1670.

Madisen L, Zwingman TA, Sunkin SM, Oh SW, Zariwala HA, Gu H, Ng LL, Palmiter RD, Hawrylycz MJ, Jones AR, et al. 2010. A robust and high-throughput Cre reporting and characterization system for the whole mouse brain. Nat Neurosci. 13:133–140.

Magistretti PJ, Cardinaux JR, Martin JL. 1998. VIP and PACAP in the CNS: regulators of glial energy metabolism and modulators of glutamatergic signaling. Ann NY Acad Sci. 865:213–225.

Markram H, Toledo-Rodriguez M, Wang Y, Gupta A, Silberberg G, Wu C. 2004. Interneurons of the neocortical inhibitory system. Nat Rev Neurosci. 5:793–807.

McBain CJ, Fisahn A. 2001. Interneurons unbound. Nat Rev Neurosci. 2:11–23.

Miyoshi G, Hjerling-Leffler J, Karayannis T, Sousa VH, Butt SJ, Battiste J, Johnson JE, Machold RP, Fishell G. 2010. Genetic fate mapping reveals that the caudal ganglionic eminence produces a large and diverse population of superficial cortical interneurons. J Neurosci. 30:1582–1594.

Morrison JH, Magistretti PJ, Benoit R, Bloom FE. 1984. The distribution and morphological characteristics of the intracortical VIP-positive cell: an immunohistochemical analysis. Brain Res. 292:269–282.

Muñoz W, Rudy B. 2014. Spatiotemporal specificity in cholinergic control of neocortical function. Curr Opin Neurobiol. 26: 149–160.

Peters A, Harriman KM. 1988. Enigmatic bipolar cell of rat visual cortex. J Comp Neurol. 267:409–432.

Pfeffer CK, Xue M, He M, Huang ZJ, Scanziani M. 2013. Inhibition of inhibition in visual cortex: the logic of connections between molecularly distinct interneurons. Nat Neurosci. 16:1068–1076.

Pi HJ, Hangya B, Kvitsiani D, Sanders JI, Huang ZJ, Kepecs A. 2013. Cortical interneurons that specialize in disinhibitory control. Nature. 503:521–524.

Poorthuis RB, Enke L, Letzkus JJ. 2014. Cholinergic circuit modulation through differential recruitment of neocortical interneuron types during behaviour. J Physiol. 592:4155–4164.

Porter JT, Cauli B, Staiger JF, Lambolez B, Rossier J, Audinat E. 1998. Properties of bipolar VIPergic interneurons and their excitation by pyramidal neurons in the rat neocortex. Eur J Neurosci. 10:3617–3628.

Porter JT, Cauli B, Tsuzuki K, Lambolez B, Rossier J, Audinat E. 1999. Selective excitation of subtypes of neocortical interneurons by nicotinic receptors. J Neurosci. 19:5228–5235.

Porter JT, Johnson CK, Agmon A. 2001. Diverse types of interneurons generate thalamus-evoked feedforward inhibition in the mouse barrel cortex. J Neurosci. 21:2699–2710.

Pouille F, Scanziani M. 2001. Enforcement of temporal fidelity in pyramidal cells by somatic feed-forward inhibition. Science. 293:1159–1163.

Rudy B, Fishell G, Lee S, Hjerling-Leffler J. 2011. Three groups of interneurons account for nearly 100% of neocortical GABAergic neurons. Dev Neurobiol. 71:45–61.

Schubert D, Kotter R, Luhmann HJ, Staiger JF. 2006. Morphology, electrophysiology and functional input connectivity of pyramidal neurons characterizes a genuine layer Va in the primary somatosensory cortex. Cereb Cortex. 16:223–236.

Staiger JF, Bojak I, Miceli S, Schubert D. 2014. A gradual depth-dependent change in connectivity features of supragranular pyramidal cells in rat barrel cortex. Brain Struct Funct. doi:10.1007/s00429–014-0726-8.

Staiger JF, Flagmeyer I, Schubert D, Zilles K, Kotter R, Luhmann HJ. 2004a. Functional diversity of layer IV spiny neurons in rat somatosensory cortex: quantitative morphology of electrophysiologically characterized and biocytin labeled cells. Cereb Cortex. 14:690–701.

Staiger JF, Masanneck C, Schleicher A, Zuschratter W. 2004b. Calbindin-containing interneurons are a target for VIP-immunoreactive synapses in rat primary somatosensory cortex. J Comp Neurol. 468:179–189.

Staiger JF, Zilles K, Freund TF. 1996. Innervation of VIP-immunoreactive neurons by the ventroposteromedial thalamic

nucleus in the barrel cortex of the rat. J Comp Neurol. 367:194–204.

Taniguchi H, He M, Wu P, Kim S, Paik R, Sugino K, Kvitsiani D, Fu Y, Lu J, Lin Y, et al. 2011. A resource of Cre driver lines for genetic targeting of GABAergic neurons in cerebral cortex. Neuron. 71:995–1013.

Thome C, Kelly T, Yanez A, Schultz C, Engelhardt M, Cambridge SB, Both M, Draguhn A, Beck H, Egorov AV. 2014. Axon-carrying dendrites convey privileged synaptic input in hippocampal neurons. Neuron. 83:1418–1430.

von Engelhardt J, Eliava M, Meyer AH, Rozov A, Monyer H. 2007. Functional characterization of intrinsic cholinergic interneurons in the cortex. J Neurosci. 27:5633–5642.

Wehr M, Zador AM. 2003. Balanced inhibition underlies tuning and sharpens spike timing in auditory cortex. Nature. 426:442–446.

Wouterlood FG, Aliane V, Boekel AJ, Hur EE, Zaborszky L, Barroso-Chinea P, Härtig W, Lanciego JL, Witter MP. 2008. Origin of calretinin-containing, vesicular glutamate transporter 2-coexpressing fiber terminals in the entorhinal cortex of the rat. J Comp Neurol. 506:359–370.

Xu X, Callaway EM. 2009. Laminar specificity of functional input to distinct types of inhibitory cortical neurons. J Neurosci. 29:70–85.

Xu X, Roby KD, Callaway EM. 2010. Immunochemical characterization of inhibitory mouse cortical neurons: three chemically distinct classes of inhibitory cells. J Comp Neurol. 518:389–404.

Zeisel A, Munoz-Manchado AB, Codeluppi S, Lonnerberg P, La Manno G, Jureus A, Marques S, Munguba H, He L, Betsholtz C, et al. 2015. Brain structure. Cell types in the mouse cortex and hippocampus revealed by single-cell RNA-seq. Science. 347:1138–1142.

Zhang S, Xu M, Kamigaki T, Hoang Do JP, Chang WC, Jenvay S, Miyamichi K, Luo L, Dan Y. 2014. Selective attention. Long-range and local circuits for top-down modulation of visual cortex processing. Science. 345:660–665.